

# DESIGN OF CORONAGRAPH FOR THE OBSERVATION OF BEAM HALO AT LHC

T. Mitsuhashi<sup>#</sup>, KEK, Ibaraki, Japan

E. Bravin, R. Jones, F. Roncarolo, H. Schmickler, G. Trad, CERN, Geneva, Switzerland

## Abstract

An observation of the beam halo using the coronagraph is planned in LHC in two phases. In the first phase, a coronagraph is designed using some optical components of the coronagraph constructed in KEK in 2005. The diffraction and Mie-scattering backgrounds from optical components near the coronagraph are analysed. Result of this analysis, we can observe a beam halo with a contrast of  $10^{-4}$  range to the peak intensity of beam core. The coronagraph is under construction and will be finished by the end of 2015.

## INTRODUCTION

In the LHC, the beam halo can lead to an important beam loss. Measurement of the beam halo distribution is therefore important for understanding and controlling the beam halo. The coronagraph is a spatial telescope to observe the sun-corona by an artificial eclipse [1]. The concept of this apparatus is to block the glare of central image and to observe a hidden image such as the sun-corona. We applied this concept for the observation of the surrounding structure (halo, tail) of the beam core. For this purpose, a coronagraph was constructed at Photon Factory, KEK in 2005 [2]. The project of using the coronagraph for the observation of beam halo image in the LHC will be performed in two phases. We plan an observation test in the first phase where the coronagraph is designed and constructed by modifying the optical design of the KEK coronagraph. This coronagraph is aiming for a halo observation with  $10^3$  to  $10^4$  contrast to the beam core, and will be set in B2 optical monitor line. In the second phase an optimum coronagraph will be designed for the LHC, to reach  $10^5$  to  $10^6$  contrast. The optical design and diffraction analysis of the coronagraph for phase 1 is described in this paper. Also Mie-scattering from lens surface or optical component in front of the objective lens is discussed and analysed.

## THE CORONAGRAPH

The coronagraph was first developed by Lyot for the observation of sun corona without waiting for an eclipse [1]. The optical layout of the coronagraph is illustrated in Fig. 1. The first lens (objective lens) makes a real image of the object (beam image) onto a blocking disk which makes artificial eclipse. The second lens (field lens), located just after the blocking disk, makes a real image of the objective lens pupil onto a mask (Lyot Stop).

The diffraction fringes are re-diffracted by the field lens aperture and transferred to the diffraction fringes on the focal plane of the field lens. The Lyot's genius idea of the coronagraph is to remove the majority of this diffraction fringes by a mask (Lyot stop), and relay the hidden image by a third lens onto final observation plane. By applying a very well polished lens for the objective, we can observe the hidden image with very high contrast (Sun corona has  $10^5$  contrast to the photosphere). With this coronagraph, we can observe a hidden image surrounding from the bright image of beam core.

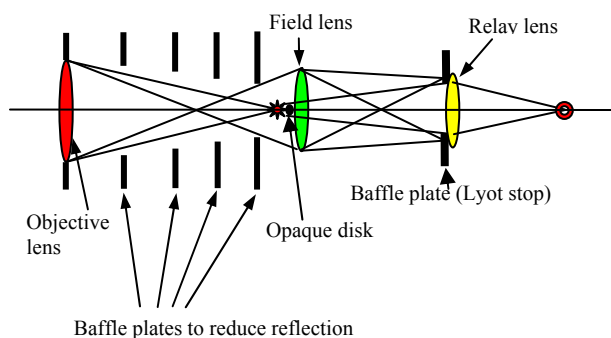


Figure 1: Layout of optical system of the coronagraph.

## OPTICAL DESIGN OF CORONAGRAPH FOR PHASE 1

For the first phase, we modified the optical design of coronagraph which was constructed in Photon Factory (PF) in 2005 in KEK [2]. The previous design of the coronagraph is optimized for the conditions at PF as listed in table 1. The same conditions of optical monitor line in B2 of LHC are also listed in table 1.

Table 1: Conditions for Design the Coronagraph at PF and LHC

	PF (BL28)	LHC(B2)
Distance between source point and objective lens	8m	28.5m
Horizontal beam size ( $1\sigma$ of beam core)	263 $\mu$ m	270 $\mu$ m
Vertical beam size ( $1\sigma$ of beam core)	80 $\mu$ m	350 $\mu$ m
Minimum size of opaque disk against beam core	6 $\sigma$ of beam core	5 $\sigma$ of beam core

Modification points of the optical design are 1) the transverse magnification reduction of the objective lens caused by the long distance between the SR source point and the objective lens, 2) Redesigning the re-diffraction system to obtain a larger image of the objective lens for a

convenient Lyot stop size, 3) Redesigning the relay system to obtain enough transverse magnification of the halo image for a convenience of observation with CCD. The optical design of previous coronagraph and new one are listed in table 2.

Table 2: The Optical Design of Previous and New Coronagraph

	PF (BL28)	LHC(B2)
Focal length of objective lens	2000mm	2000mm
Objective lens aperture	50 x 50mm	25 x 25 mm
Transverse magnification	0.333	0.0754
Opaque disk size	1mm	0.110mm
Focal length of field lens	500mm	800mm
Movable range of Lyot stop	2 x 2mm to 20 x 20mm	2 x 2mm to 20 x 20mm
Focal length of relay lens	36mm	500mm

### DIFFRACTION ANALYSIS

The aperture of the objective lens causes the diffraction fringes surrounding from the central image. The disturbance of the diffraction pattern of the first objective lens aperture is given by the Fraunhofer diffraction of the entrance pupil as follows:

$$F(\xi, \eta) = \frac{1}{i \cdot \lambda \cdot f_{obj}} \int f_{obj}(x, y) \exp\left\{-\frac{i \cdot 2 \cdot \pi \cdot (x \cdot \xi + y \cdot \eta)}{\lambda \cdot f_{obj}}\right\} dx dy$$

In here,  $f_{obj}(x, y)$  is inout disturbance to entrance pupil and  $f_{obj}$  is denotes the distance between the objective lens and its imaging plane. For a rectangular shape aperture, this Fourier transform results a sinc function. The result of calculation for the cross section of diffraction intensity by the objective lens is shown in Fig. 2.

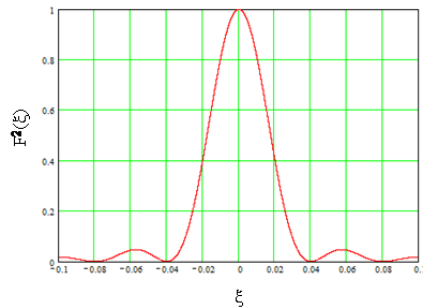


Figure 2: Intensity of diffraction pattern by objective lens pupil.

The diffraction pattern by next field lens on Lyot stop is given by Fourier transform of the disturbance  $F(\xi, \eta)$  on the field lens pupil. The field lens pupil is defined by both its outer aperture and the opaque disk. The input disturbance of the light for this pupil is the diffraction fringes without the airy disk in the diffraction pattern of objective lens. This disturbance is diffracted again with re-diffraction system, and resulting diffraction fringes on

the imaging plane of the field lens. Using Babinet's principle [3], the disturbance of re-diffracted light  $F_{field}(X)$  on the imaging plane of the field lens is given by,

$$F_{field}(X, Y) = \frac{1}{i \cdot \lambda \cdot f_{field}} \left[ \int_0^{\xi_2} F(\xi, \eta) \exp\left\{-\frac{i \cdot 2 \cdot \pi \cdot (\xi \cdot X + \eta \cdot Y)}{\lambda \cdot f_{field}}\right\} d\xi d\eta \right] - \int_0^{\xi_1} F(\xi, \eta) \exp\left\{-\frac{i \cdot 2 \cdot \pi \cdot (\xi \cdot X + \eta \cdot Y)}{\lambda \cdot f_{field}}\right\} d\xi d\eta$$

Where  $\lambda$  denotes wavelength of input light,  $\xi_1$  denotes radius of stop,  $\xi_2$  denotes the aperture radius at the field lens pupil and  $f_{field}$  denotes the distance between the field lens and its imaging plane (location of Lyot stop), respectively. The result of calculation for the cross section of intensity distribution  $|F^2(X)|$  using a square-pupil at the objective lens is shown in Fig. 3.

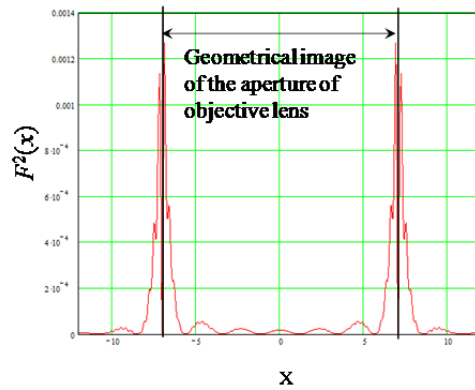


Figure 3: Intensity distribution  $|F_{field}^2(X)|$  on imaging plane of field lens.

From this figure, we can see the majority of diffraction fringes located in the inside and outside of the geometrical image of the objective lens edge (it is called the Schlieren image of objective lens edge). Blocking this majority of diffraction fringes with a mask (Lyot Stop), prevents most of the diffraction fringes light from reaching later stages of the coronagraph. Since the width of the two diffraction fringes is inverse proportional to the opaque disk diameter, increasing the latter reduces the light leakage from the diffraction fringe inside of Lyot stop.

A diffraction pattern on the imaging plane of the relay lens is produced by the remaining disturbance of light inside of Lyot stop. This diffraction pattern is given by an Fourier transform of the disturbance  $F_{field}(\xi, \eta)$  in the field lens pupil (Opening of the Lyot stop),

$$F_i(\xi, \eta) = \frac{1}{i \cdot \lambda \cdot f_{field}} \int F_{field}(x, y) \exp\left\{-\frac{i \cdot 2 \cdot \pi \cdot (X \cdot X_i + Y \cdot Y_i)}{\lambda \cdot f_{field}}\right\} dX dY$$

This is the diffraction background in the coronagraph. A result of calculation for the diffraction pattern by relay lens pupil is shown in Fig. 4, where the peak intensity of this diffraction fringe is  $3.7 \times 10^{-4}$ . Except of the two central fringes, most of diffraction fringes have intensities ranging from  $10^{-5}$  to  $10^{-6}$  range. In the usual condition of the coronagraph, the opaque disc diameter is in the range

of few mm [2], resulting a diffraction background of  $10^{-6}$  to  $10^{-7}$  range. In the present case, the diffraction fringes eliminated by Lyot stop is wider corresponding to small opaque disk diameter as shown in Fig. 3, thus the leakage of diffraction fringe light becomes larger.

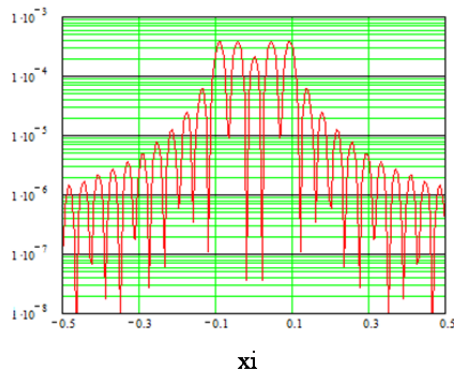


Figure 4: Intensity of diffraction pattern on imaging plane of relay lens.

### BACKGROUND NOISE DUE TO MIE-SCATTERING

After blocking the central bright core image and cutting the light from the diffraction fringes, we still have some scattered light noise from the objective lens of the coronagraph. The defects in the objective lens such as scratches and digs on its surface and some defects on the optical components such as mirrors in near front of the objective lens and dust in air will produce the Mie-scattering. The intensity of these Mie-scattered lights possibly reaches the  $10^{-3}$  order. In this chapter, we discuss a diffraction treatment of the Mie-scattering.

Let us approximate the  $i$ -th noise source in the pupil as an opaque disk having a diameter of  $r_0$  as shown in Fig. 5.

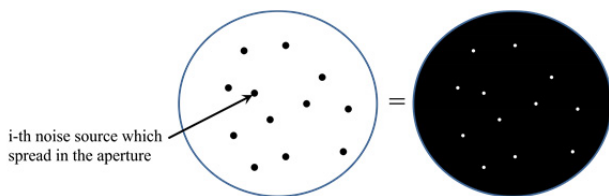


Figure 5: The pupil with Mie scattering sources.

Using the Babinet's principle again [4], the pupil is given by reversing the contrast and its function is expressed by,

$$P_i(r_0, x, y) = -\text{circ}(r_0, x, y)$$

$$P(\bar{r}, x, y) = \sum_i P_i(r_0, x, y) \cdot \exp(-ik(x_i + y_i))$$

When the distance between the opaque disks is assumed to be longer than the transverse coherent length, the pupil function becomes,

$$P(\bar{r}, x, y) = \sum_i P_i(r_0, x, y)$$

### Case 1 Mie-scattering Source on the Objective Lens

First we consider the case where the Mie-scattering sources are on the objective lens. A sketch of this case is shown in Fig. 6.

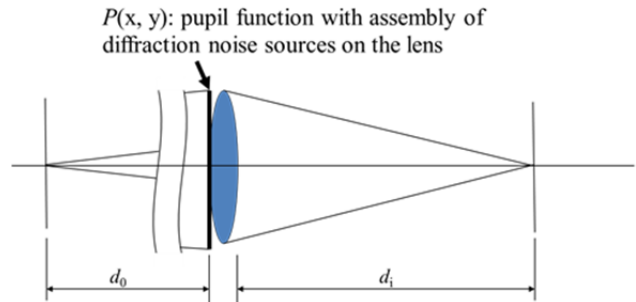


Figure 6: Case 1, Mie-scattering sources on the objective lens.

The impulsive response on the image plane is then given by,

$$h(x_i, y_i; x_0, y_0) = \frac{1}{\lambda d_0 d_i} \iint P(\bar{r}, x, y) \exp\left\{-i \frac{2\pi}{\lambda d_i} [(x_i + Mx_0)x + (y_i + My_0)y]\right\} dx dy$$

where  $M = d_i / d_0$  denotes the geometrical magnification. This result means Mie-scattering from small opaque disk on the objective lens is given by the Fraunhofer diffraction of the holes. Since the diffraction intensity is inverse-proportional to the following extinction rate,

$$\text{Extinction rate} = \frac{\text{entrance pupil aperture area}}{\text{total area of noise source}}$$

the total intensity of Mi-scattering against diffraction intensity by lens pupil is scaled by this extinction rate.

### Case 2 Mie-scattering Sources in Front of Objective Lens

In the following, we consider the pupil which has the Mie-scattering source in front of the objective lens as shown in Fig. 7.

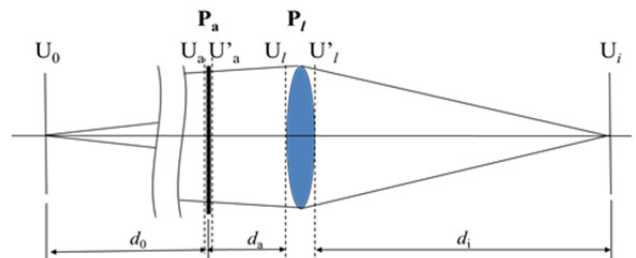


Figure 7: Case 2, Mie-scattering source in front of objective lens.

This is the case of some optical components such as the mirror in front of the objective lens. Since the disturbance

of light  $U_a'$  after the pupil  $P_a$  propagates in free space reaching the front of the objective lens,  $U_1$  is given by Fresnel transfer of  $U_a'$ . When passing through the lens, the disturbance  $U_1$  is given by the lens transfer of  $U_1$ . Finally the disturbance on the imaging plane  $U_i$  is given by Fresnel transfer of  $U_1'$ . The result of these calculations is given by,

$$U_i(x_i, y_i) = \iint \left[ \iint P_a(x_a, y_a) \exp \left\{ i \frac{k}{2} \left( \frac{1}{d_0 - d_a} - \frac{1}{d_a} \right) (x_a^2 + y_a^2) \right\} \cdot \exp \left\{ -ik \left( \left( \frac{x_0}{d_0 - d_a} + \frac{x_i}{d_a} \right) x_a + \left( \frac{y_0}{d_0 - d_a} + \frac{y_i}{d_a} \right) y_a \right) \right\} dx_a dy_a \right] \cdot P_l(x_i, y_i) \exp \left\{ i \frac{k}{2} \left( \frac{1}{d_i} + \frac{1}{d_l} - \frac{1}{f} \right) (x_i^2 + y_i^2) \right\} \cdot \exp \left\{ -i \frac{k}{d_i} (x_i x_i + y_i y_i) \right\} dx_i dy_i$$

The first double integral originates from the diffraction of Mie-scattering source while the second double integral results from the diffraction of lens pupil.

*Actual Mie Scattering Source on the Surface of Optical Component*

A photograph of a surface with the optical polishing quality of scratch & dig 60/40 is shown in Fig. 8 [2]. The optical surface quality 60/40 guarantees no larger scratches than 6µm width, and no larger dig than 400µm. The side of this photograph is 5mm. This photograph is taken with the dark field illumination method. The surface with optical polishing “scratch & dig 60/40” still has many digs (small shiny spots in the photograph).

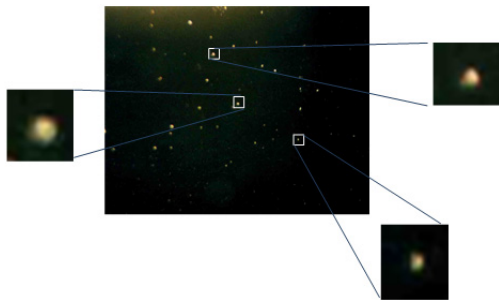


Figure 8: A photograph of surface with the optical polishing quality of scratch & dig 60/40. The side of this picture is 5mm.

Actually, no recognisable scratch can be found on this surface, and the maximum diameter of dig is about 100µm.

*Simulation of Mie-scattering Background from Lens Surface*

Results of simulation of the Mie-scattering background for dig diameters of 400µm, 200µm, 100µm, 50µm on the imaging plane of objective lens are shown with the diffraction of objective lens pupil in Fig. 9. The diffraction patterns are shown for field of ±10mm on the imaging plane of the objective lens. The dig diameter of

400µm corresponds to the maximum possible size in dig 40. In this simulation, an extinction ratio corresponding to number of dig 20digs/5mm<sup>2</sup> was assumed. A zoom-up plot of the diffraction patterns for a significant field is shown in Fig. 10. This field corresponds to 20σ of the beam core size, and a significant beam halo image will be appeared in this field.

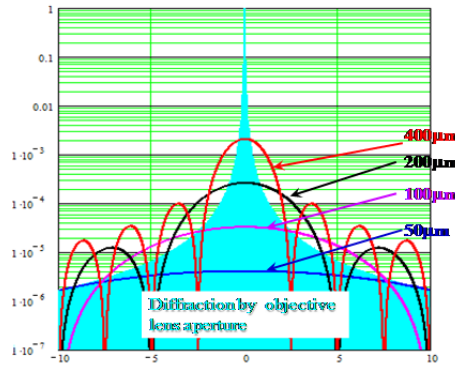


Figure 9: Results of simulation of Mie-scattering background for dig diameter of 400µm, 200µm, 100µm, 50µm on imaging plane of the objective lens with the diffraction of objective lens pupil.

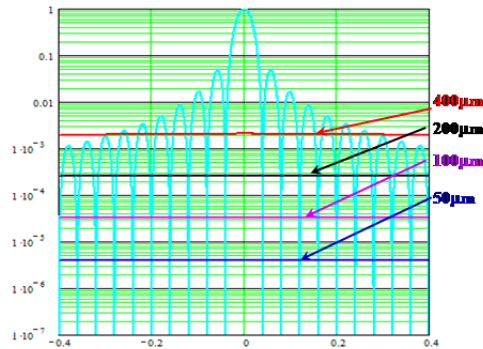


Figure 10: A zoom up plot of diffraction patterns.

According to Fig. 9, the Mie-scattering intensity corresponding to 400µm dig has an intensity of  $2 \times 10^{-3}$  of the peak intensity of the objective lens diffraction. Moreover, a  $3 \times 10^{-4}$  peak is found for a 200µm dig,  $3 \times 10^{-5}$  for 100µm dig and  $4 \times 10^{-6}$  for 50µm dig respectively. The Mie-scattering background can be an important contribution to the overall coronagraph background.

*Example of Observation of Mie-scattering Noise*

An example of Mie-scattering background observation is shown in Fig. 11 [2], where in (a) a result of beam halo observation in PF is found while in (b) same image taken with some intentionally sprayed dust onto a mirror located 1m in front of the objective lens. In this example, the beam halo image is totally hidden by the bright Mie-scattering noise. This case corresponds to the Case 2, and out of focus image of noise source plus its Fresnel like diffraction due to a shorter  $D_0$ .

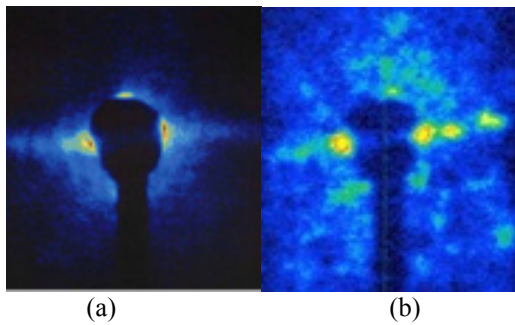


Figure 11: Observation of Mie-scattering noise in beam halo observation at PF. Observed beam halo at PF (a), same image taken with some intentionally sprayed dust onto a mirror located 1m in front of the objective lens (b).

## ARRANGEMENT OF CORONAGRAPH SETUP IN B2 OPTICAL HUT

The coronagraph layout is proposed to fit in the SR monitor hut of B2 in the LHC. The objective lens of the coronagraph which is constructed in PF [2] is reused for phase 1 LHC coronagraph. However, the rest of the optical system is redesigned. The optical hut has 4.8m x 0.8m optical table housing an imaging line and a calibration. To fit in the coronagraph, the calibration line will be dismantled and the imaging line rearranged. A proposed rearrangement on the optical table is shown in Fig. 12. Due to a limitation of the length of the optical table, and long length of the coronagraph, the coronagraph optical axis is folded two times by 90 degrees after the field lens (this tilting in the coronagraph is very common due to their long length). The existing imaging line will be set surrounding the coronagraph.

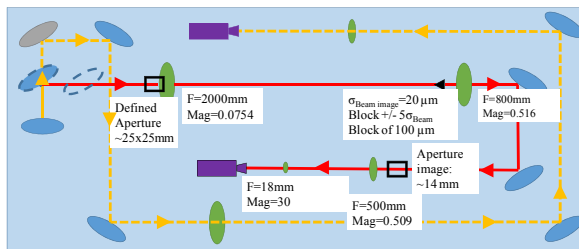


Figure 12: Arrangement of the coronagraph on the optical table at B2.

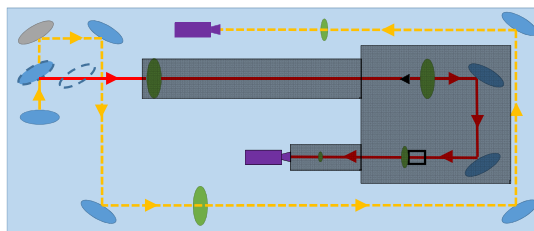


Figure 13 Surrounding tubes and dark box.

In this arrangement, we have three relay mirrors set in front of the objective lens: the in-vacuum SR extraction mirror followed by an optical widow for separation of the vacuum and two steering mirrors. Surfaces on these

ISBN 978-3-95450-176-2

optical components can serve as the Mie-scattering noise sources. The optical components of the coronagraph will be covered with surrounding tubes in a dark box to escape from external parasitic light noise and also to reduce the air turbulence of in long optical path. The layout of the coronagraph surrounding structure is shown in Fig. 13.

## SUMMARY

Coronagraph optics for phase 1 observation of beam halo is designed for B2 SR monitor beam line at LHC. From diffraction analysis, the background in this coronagraph from leakage of diffraction fringe is estimated to be  $3.7 \times 10^{-4}$ . The diffraction fringes from the relay lens square aperture is mainly localized in the horizontal and vertical medium plane, we possibly can distinguish beam halo image between diffraction fringes by rotating the aperture pupil. Since the existing B2 SR line is not optimised for coronagraph observation, the performance of coronagraph will also be limited by the Mie-scattering noise from existing optical components such as mirrors. On the surface of actual optical components with scratch & dig of 60/40, the  $400\mu\text{m}$  dig is very rare. The digs having a diameter smaller than  $100\mu\text{m}$  are the majority. For this reason, an order of  $10^{-4}$  to  $10^{-5}$  background can be expected for phase 1 using the B2 SR monitor line. The Mie-scattering noise from small digs is almost flat distribution over the significant field as shown in Fig. 10, we have a possibility to subtract this background. We expect to observe the beam halo with a contrast of  $10^4$  using coronagraph set in B2. Actual arrangement of coronagraph on B2 optical table is also studied. The designed coronagraph is now under construction and should be ready by the end of 2015.

## LODESTER FOR PHASE 2 CORONAGRAPH DESIGN

The background is caused by from diffraction fringe leakage in Lyot stop that limits the theoretical contrast in the coronagraph. Since leakage of diffraction fringe is reduced by increasing the opaque disk diameter, we can achieve a better contrast by increasing the beam core image size. Therefore we should design the focal length of the objective lens. Since the chromatic shift on the optical axis is given by the focal length divided by the Abbe number, designing a long focal length implies increasing the chromatic focal shift. Reflector focusing system for the objective should be considered instead of the objective lens system in stage 2. Actually, recent space coronagraph such as LASCO coronagraph [4] applied reflective system for objective system.

## REFERENCES

- [1] B.F. Lyot. *Notice Roy. Ast. Soc.*, p580, **99** (1939).
- [2] T. Mitsuhashi, *Proc. Of DIPAC 2005*, p7 (2005) Lyon.
- [3] G.E. Bruecknere, et al., *Solar Physics*, **162**, p357 (1995)
- [4] M. Born and E. Wolf, "Principal of Optics", p424, 7<sup>th</sup> ed., Cambridge University Press (1999).